LDH Nanocomposites with Different Guest Entities as Precursors of Supported Ni Catalysts

Corine Gérardin, Dessislava Kostadinova, Bernard Coq, and Didier Tichit*

Institut Charles Gerhardt UMR 5253 CNRS/UM2/ENSCM/UM1, Matériaux Avancés pour la Catalyse et la Santé, 8 rue Ecole Normale, 34296 Montpellier Cedex 5, France

Received May 3, 2007. Revised Manuscript Received January 7, 2008

Nanocomposites built by intercalation of negatively charged Ni hydroxy citrate species $[Ni(C_6O_7H_3)_x(OH)]_y^{y(3x-1)-}$ and $NiCl_4^{2-}$ guest entities in the interlayer space of host Mg/Al layered double hydroxides (LDHs) have been obtained by anionic exchange. The sizes of the Ni particles in the Ni/Mg(Al)O samples formed by thermal reduction in H_2 of these precursors as well as the reconstruction abilities of the mixed oxides in water have been examined. The Ni complexation ratio $x = [C_6O_7H_3]/[Ni]$ in the $[Ni(C_6O_7H_3)_x(OH)]_y^{y(3x-1)-}$ clusters has been varied from 0.5 to 2 giving rise to a series of LDH composites with different Ni contents. As x increases, the mean negative charge per Ni atom of the intercalated anionic species indeed increases, and the Ni content in the nanocomposites concurrently decreases from 15 to 7 wt %. The mean size of the Ni^0 crystallites varies with the reduction temperature and the composition of the guest entities in the $[Ni(C_6O_7H_3)_x(OH)]_y^{y(3x-1)-}$−LDH nanocomposites as shown by XRD and TEM analyses. The mean size of the Ni^0 crystallites decreases from approximately 10 to 5 nm after reduction at 600 °C when x increases from 0.6 to 2. This is consistent with the decrease of the average size of the Ni hydroxy citrate colloids in solution. It is shown that the size of the colloids in the precursors allows the size of the Ni^0 particles in the final Ni^0/Mg(Al)O material to be controlled. When $NiCl_4^{2-}$ is used as the guest entity, Ni particles obtained after reduction are larger. The Mg(Al)O supports behave very differently in the two types of reduced nanocomposites upon reconstruction in water. The layered structure is restored when the guest entity is $NiCl_4^{2-}$ in the precursor, but in contrast Mg(Al)O is highly stabilized when it is $[Ni(C_6O_7H_3)_x(OH)]_y^{y(3x-1)-}$. A strong interaction between the embedded Ni particles and Mg(Al)O prevents reconstruction in the latter case. The segregation of large particles in the former makes Mg(Al)O rehydration easier.

1. Introduction

Nanocomposites built from an assembly of a layered double hydroxide (LDH) host structure and different types of anionic guest entities attract considerable interest because of the wide range of applications. LDHs of general formula $[M_{1-x}^{2+}M_x^{3+}(OH)_2][A_{x/n}^{n-}\cdot mH_2O]$ contain different M^{2+} and M^{3+} metal cations in their brucite-like sheets and various A^{n-} charge-compensating anions in their interlayer space. Anionic guest entities like monomers and polymers,[1,2] functional biomolecules,[3–7] and complexes of reducible transition metals[8–12] have been intercalated within an LDH matrix. LDH nanocomposites thus obtained found applications in mechanical strengthening[1,2] and drug delivery[3,7] and as adsorbents,[13] membranes,[14] or magnetic nanostructures;[8–12] in contrast, their potentialities as homogeneous and heterogeneous catalysts have been scarcely explored.

The behavior of stabilized homogeneous catalytic moieties prepared from intercalation into LDH was mainly explored to date. It is indeed the case for a variety of biomimetic oxidation catalysts, for example, porphyrins and Co phthalocyanines, whose activities in oxidation reactions were improved after intercalation.[15] Oxomolybdenum complexes, active in the oxidation of thiols, deactivate by formation of a dimer; this is prevented when complexes are intercalated

* Corresponding author. E-mail: didier.tichit@enscm.fr. Phone: 33(0)4 67 16 34 77. Fax: (0)4 67 16 34 70.

(1) Leroux, F.; Taviot-Guého, C. *J. Mater. Chem.* **2005**, *15*, 3629.
(2) Darder, M.; Lopez-Blanco, M.; Aranda, P.; Leroux, F.; Ruiz-Hitzky, E. *Chem. Mater.* **2005**, *17*, 1969.
(3) Ambrogi, V.; Fardella, G.; Grandolini, G.; Perioli, L. *Int. J. Pharm.* **2001**, *220*, 22.
(4) Choy, J. H.; Kwak, S. Y.; Jeong, Y. J.; Park, J. S. *Angew. Chem., Int. Ed.* **2000**, *39*, 4042.
(5) Del Arco, M.; Cebadera, E.; Gutierrez, S.; Martin, C.; Montero, M. J.; Rives, V.; Rocha, J.; Sevilla, M. A. *J. Pharm. Sci.* **2004**, *93*, 1649.
(6) Choy, J. H.; Jung, J. S.; Oh, J. M.; Park, M.; Jeong, J.; Kang, Y. K.; Han, O. J. *Biomater.* **2004**, *25*, 3059.
(7) Nakayama, H.; Wada, N.; Tsuhako, M. *Int. J. Pharm.* **2004**, *269*, 469.
(8) Tarasov, K. A.; Isupov, V. P.; Bokhonov, B. B.; Gaponov, Y. A.; Tolochko, B. P.; Sharafutdinov, M. R.; Shatskaya, S. S. *J. Mater. Synth. Process.* **2000**, *8*, 21.
(9) Tarasov, K. A.; Isupov, V. P.; Yulikov, M. M.; Yermakov, A. E.; O'Hare, D. *Solid. State Phenom.* **2003**, *90*, 527.
(10) Tarasov, K. A.; O'Hare, D.; Isupov, V. P. *Inorg. Chem.* **2003**, *42*, 1919.
(11) Nikivorov, M. P.; Chernysheva, M. V.; Eliseev, A. A.; Lukashin, A. V.; Tretyakov, Y. D.; Maksimov, Y. V.; Suzdalev, I. P.; Goernert, P. *Mater. Sci. Eng., B* **2004**, *109*, 226.
(12) Tsyganok, A.; Sayari, A. *J. Solid State Chem.* **2006**, *179*, 1830.
(13) Dékány, I.; Berger, F.; Imrik, K.; Lagaly, G. *Colloid Polym. Sci.* **1997**, *275*, 681.
(14) Hornok, V.; Erdõhelyi, A.; Dékány, I. *Colloid Polym. Sci.* **2005**, *283*, 1050.
(15) Auer, S. M.; Grunwaldt, J. D.; Köppel, R. A.; Baiker, A. *J. Mol. Catal. A* **1999**, *139*, 305.
(16) Cervilla, A.; Corma, A.; Fornés, V.; Llopis, E.; Palanca, P.; Rey, F.; Ribera, A. *J. Am. Chem. Soc.* **1994**, *116*, 1595.
(17) Corma, A.; Fornés, V.; Rey, F.; Cervilla, A.; Llopis, E.; Ribera, A. *J. Catal.* **1995**, *152*, 237.

10.1021/cm071194l CCC: $40.75
Published on Web 02/20/2008

within LDH.[16,17] Molybdate species intercalated into LDH are highly efficient epoxidation and bromination catalysts.[18,19]

The most widespread route to elaborate supported metal catalysts from LDH involves the calcination and/or reduction of LDH containing framework transition metal.[20–26] The obtained catalysts usually exhibit peculiar metal−support interaction ("electron transfer") or metal−support cooperation ("metal−base bifunctional catalysis").[27] This approach has been extensively developed in the case of Ni-based catalysts.[23–25,28–30] However, it must be underlined that the decomposition of multicationic LDH generally fails to elaborate small metal particles at high metal loadings. Therefore, alternative routes were considered to achieve higher Ni dispersion from LDH precursors.[31] Among them, the exchange in the interlayer space of anionic guest species has attracted special attention. Such interest was prompted because anionic multinuclear guest species can be introduced with a fine control of the nuclearity, and *in fine* of the particle size. In the case of LDH, some examples can be found with the exchange of $NiCl_4^{2-}$,[32,33] $[Ni(Edta)]^{2-}$,[8,10,12,34] and $[Ni(C_6O_7H_3)(OH)]^{2-}$.[35] In the latter case we have demonstrated that when the degree of exchange with these anionic clusters increases in the LDH the Ni loading increases from 8 to 15%.[35] As citrate ions are strong complexing agents, one may anticipate that the citrate/Ni ratio also influences the nuclearity and size of the clusters. This is one of the aspects we intend to tackle in the present work.

For applications in catalysis, Ni-LDH nanocomposites are thermally treated and usually transform into Ni^0/Mg(Al)O metal supported catalysts. Because in many cases Ni^0/Mg(Al)O will be in contact with water in the course of the catalytic process, reconstruction of the Mg(Al)O mixed oxide into the LDH structure may occur. This reconstruction phenomenon has been put forward in applications of Pd- and Ni-containing LDHs and induces some modifications of the catalytic properties.[36–38] Several reports show that reconstruction of Mg(Al)O into the Mg/Al-LDH structure is affected by the presence of transition metals, with *in fine* some modifications of the catalytic properties.[34,37,38] Because the introduction of metal particles within LDH by means of colloids is a novel approach to access Mg(Al)O supported metal catalysts, a second aspect of this work was aimed at investigating reconstruction of these materials.

To sum up, this work is devoted to the study of Ni-LDH composites elaborated by intercalation of $[Ni(C_6O_7H_3)_x(OH)]_y^{y(3x-1)-}$ clusters with a focus on (i) the fine tuning of Ni^0 particle size and loading through the citrate/Ni ratio and (ii) the ability of LDH reconstruction. Comparison will be made with materials elaborated by intercalation of $NiCl_4^{2-}$.

2. Experimental Section

2.1. Preparation of Ni Colloids. Colloidal suspensions of Ni-based particles were obtained by hydrolysis of Ni citrate complexes, which were previously prepared. First, aqueous solutions of $Ni(NO_3)_2 \cdot 6H_2O$ (0.5 M) and $Na_3C_6O_7H_3$ were mixed according to a molar complexation ratio $[C_6O_7H_3]/[Ni]$, which was varied between 0.5 and 2. Then hydrolysis of Ni^{2+} ions was performed by adding a 0.5 M NaOH solution with a controlled nickel hydroxylation ratio $[OH]/[Ni] = 1$. That led to stable colloidal suspensions of $[Ni(C_6O_7H_3)_x(OH)]_y^{y(3x-1)-}$ colloids, where y represents the number of Ni metal ions per cluster. Freshly prepared suspensions have been used for intercalation.

2.2. Preparation of HDL Host Structures and Nanocomposites. The host Mg/Al LDH (Mg/Al = 2) was prepared by coprecipitation at constant pH (≈ 10) of suitable amounts of $Mg(NO_3)_2 \cdot 6H_2O$ (0.2 M), $Al(NO_3)_3 \cdot 6H_2O$ (0.1 M) with a 1 M NaOH solution. Addition of the alkaline solution was controlled by using a pH-STAT Titrino (Metrohm) apparatus to keep the pH constant. The suspension was stirred overnight at 80 °C for 17 h, and the solid was then separated by centrifugation, thoroughly washed with distilled water (Na < 100 ppm), and dried overnight at 80 °C. This sample will be hereafter labelled NO_3-Mg/Al.

A Mg/Al LDH intercalated with citrate anions has been prepared by anionic exchange of the previous sample. The exchange was performed by equilibrating 3 g of NO_3-Mg/Al with 50 mL of a 7.4×10^{-2} M $Na_3C_6O_7H_3$ solution at 25 °C for 2 h under stirring. The solid was then separated by centrifugation, washed with distilled water, and dried overnight at 80 °C. This sample will be hereafter labelled Cit-Mg/Al.

The Ni hydroxyl citrate Mg/Al-LDH nanocomposites were prepared from the NO_3-Mg/Al LDH by anionic exchange of the nitrate ions. The host NO_3-Mg/Al LDH (3 g) was dispersed in the required amount (300–320 mL) of a $[Ni(C_6O_7H_3)_x(OH)]_y^{y(3x-1)-}$ colloidal suspension ($[Ni] = 0.03$ M; $x = [C_6O_7H_3]/[Ni] = 0.5$, 0.6, 0.7, 1, 1.5, 2), corresponding to 1.5 times the theoretical anionic exchange capacity (AEC) of the sample (3.7 mequiv g^{-1}). The exchange process was performed by stirring the mixture in air at room temperature (RT) for 12 h. The solid was then recovered, washed by dispersion and centrifugation in deionized water, and finally dried at 80 °C for 12 h. The nanocomposites were hereafter labelled Cit_xNi-Mg/Al.

A LDH nanocomposite was obtained by anion exchange with $NiCl_4^{2-}$ of the NO_3-Mg/Al host structure. The intercalation was

(18) Sels, B.; De Vos, D.; Buntinx, M.; Pierard, F.; Kirsch-De Mesmaeker, A.; Jacobs, P. *Nature* **1999**, *400*, 855.
(19) Van Laar, F. M. P. R.; De Vos, D. E.; Pierard, F.; Kirsch-De Mesmaeker, A.; Fiermans, L.; Jacobs, P. *J. Catal.* **2001**, *197*, 139.
(20) Tichit, D.; Medina, F.; Coq, B.; Dutartre, R. *Appl. Catal., A* **1997**, *159*, 241.
(21) Holgado, M. J.; Rives, V.; San Roman, M. S. *Appl. Catal., A* **2001**, *214*, 219.
(22) Monzón, A.; Romeo, E.; Royo, C.; Trujillano, R.; Labajos, F. M.; Rives, V. *Appl. Catal., A* **1999**, *185*, 53.
(23) Coq, B.; Tichit, D.; Ribet, S. *J. Catal.* **2000**, *189*, 117.
(24) Olafsen, A.; Slagtern, Å.; Dahl, I. M.; Olsbye, U.; Schuurman, Y.; Mirodatos, C. *J. Catal.* **2005**, *229*, 163.
(25) Basile, F.; Basini, L.; D'Amore, M.; Fornasari, G.; Guarinoni, A.; Matteuzzi, D.; Del Piero, G.; Trifirò, F.; Vaccari, A. *J. Catal.* **1998**, *173*, 247.
(26) Narayanan, S.; Krishna, K. *Appl. Catal., A* **1998**, *174*, 221.
(27) Tichit, D.; Coq, B. *CATTECH* **2003**, *7*, 206.
(28) Morioka, H.; Shimizu, Y.; Sukenobu, M.; Ito, K.; Tanabe, E.; Shishido, T.; Takehira, K. *Appl. Catal., A* **2001**, *215*, 11.
(29) Marquevich, M.; Farriol, X.; Medina, F.; Montané, D. *Catal. Lett.* **2003**, *85*, 41.
(30) Unnikrishnan, R.; Narayanan, S. *J. Mol. Catal. A* **1999**, *144*, 173.
(31) Tichit, D.; Gerardin, C.; Durand, R.; Coq, B. *Top. Catal.* **2006**, *39*, 89.
(32) Lopez Salinas, E.; Ono, Y. *Microporous Mater.* **1993**, *1*, 33.
(33) Okada, K.; Matsushita, F.; Hayashi, S. *Clay Miner.* **1997**, *32*, 299.
(34) Tsyganok, A. I.; Suzuki, K.; Hamakawa, S.; Takehira, K.; Hayakawa, T. *Catal. Lett.* **2001**, *77*, 75.
(35) Gérardin, C.; Kostadinova, D.; Sanson, N.; Coq, B.; Tichit, D. *Chem. Mater.* **2005**, *17*, 6473.
(36) Alcaraz, J. J.; Arena, B. J.; Gillespie, R. D.; Holmgren, J. S. *Catal. Today* **1998**, *43*, 89.
(37) Corma, A.; García, H.; Primo, A. *J. Catal.* **2006**, *241*, 123.
(38) Takehira, K.; Kawabata, T.; Shishido, T.; Murakami, K.; Ohi, T.; Shoro, D.; Honda, M.; Takaki, K. *J. Catal.* **2005**, *231*, 92.

Table 1. Compositions Obtained from Chemical Analysis, Proposed Formula, and Surface Areas of the Samples

sample	x^a	surface area^b ($m^2\ g^{-1}$)	chemical composition (wt %) Mg	Al	Ni	C	N	Cl	formula
NO_3-Mg/Al	0	101*	18.14	10.10		0.30	4.61		$[Mg_{0.67}Al_{0.33}(OH)_2][(NO_3)_{0.29}(CO_3)_{0.022}$, $0.62H_2O$
Cit-Mg/Al			17.82	10.06		8.55	0.15		$[Mg_{0.66}Al_{0.33}(OH)_2][(NO_3)_{0.13}(C_6O_7H_3)_{0.11}]$, $0.26H_2O$
$Cit_{0.5}$Ni-Mg/Al	0.5		11.15	6.29	14.73	8.21	0.68		$[Mg_{0.67}Al_{0.33}(OH)_2][(NO_3)_{0.07}(CO_3)_{0.052}[Ni(C_6O_7H_3)_{0.46}(OH)_{1.36}]_{0.36}]$, mH_2O
$Cit_{0.6}$Ni-Mg/Al	0.6	334	13.71	7.17	10.41	9.13	0.22		$[Mg_{0.68}Al_{0.32}(OH)_2][(NO_3)_{0.019}[Ni(C_6O_7H_3)_{0.72}(OH)_{1.25}]_{0.21}]$, $0.72H_2O$
$Cit_{0.7}$Ni-Mg/Al	0.7		13.69	7.44	9.20	9.17	0.29		$[Mg_{0.67}Al_{0.33}(OH)_2][(NO_3)_{0.024}[Ni(C_6O_7H_3)_{0.81}(OH)_{1.19}]_{0.18}]$, mH_2O
Cit_1Ni-Mg/Al	1	278*	14.91	7.70	7.33	9.66	0.14		$[Mg_{0.68}Al_{0.32}(OH)_2][(NO_3)_{0.011}[Ni(C_6O_7H_3)_{1.09}(OH)_{0.96}]_{0.14}]$, $0.43H_2O$
$Cit_{1.5}$Ni-Mg/Al	1.5	286	15.25	7.67	6.84	9.36	0.10		$[Mg_{0.69}Al_{0.31}(OH)_2][(NO_3)_{0.08}[Ni(C_6O_7H_3)_{1.12}(OH)_{1.03}]_{0.13}]$, mH_2O
Cit_2Ni-Mg/Al	2	305	15.03	7.76	7.25	9.33	0.10		$[Mg_{0.68}Al_{0.32}(OH)_2][(NO_3)_{0.008}[Ni(C_6O_7H_3)_{1.06}(OH)_{1.11}]_{0.13}]$, mH_2O
ClNi-Mg/Al			19.30	11.10	2.7	0.24	0.10	13.82	$[Mg_{0.66}Al_{0.34}(OH)_2][[NiCl_4]_{0.037}(NO_3)_{0.006}(CO_3)_{0.016}Cl_{0.168}]$, mH_2O

^{a} $[C_6O_7H_3]$/[Ni] molar ratio in solution. ^{b} BET specific surface area determined on samples calcined at 723 K (*calculated using the *t*-plot method).

performed according to a method previously reported.[32] For this purpose $[NiCl_4]^{2-}$ species were first obtained by dissolution of 2.81 g of $NiCl_2$ (0.022 mol) and 7.19 g of $(C_2H_5)_4NCl$ (0.044 mol) in 300 mL of ethanol and stirring for 2 h at 25 °C. This solution was then added to 4 g of NO_3-Mg/Al. The exchange was performed for 12 h at 25 °C under vigorous stirring. The solid was then recovered and dried at 80 °C for 12 h. This sample will be hereafter labelled ClNi-Mg/Al.

2.3. Elaboration of the Ni^0/Mg(Al)O Materials. The nanocomposites were firstly thermally decomposed under N_2 or air flow for 2 h at 450 °C (heating rate: 5 °C min^{-1}) and then reduced in a diluted hydrogen flow (H_2/Ar: 5/95) for 2 h at 600 or 1000 °C (heating rate: 5 °C min^{-1}).

2.4. Reconstruction of the LDH. Reconstruction experiments have been performed on the samples previously thermally decomposed in air or in a H_2/Ar flow (5/95) at 600, 800, or 1000 °C for 2 h. Rehydration was carried out in a liquid phase by dispersing 2 g of thermally treated sample in 100 mL of water under vigorous mechanical stirring during 2 h or 24 h at RT and neutral pH. After the rehydration process, the samples were filtered and dried at 80 °C for 12 h.

2.5. Characterization Techniques. Chemical analyses of both as-prepared samples and calcined materials at 450 °C were carried out by inductively coupled plasma atomic emission spectroscopy (ICP-AES) at the Central Analysis Service of the CNRS (Solaize, France).

Hydrodynamic sizes of the $[Ni(C_6O_7H_3)_x(OH)]_y^{y(3x-1)-}$ colloids were determined by dynamic light scattering at a detection angle of 90° using a Malvern Autosizer 4800 apparatus.

N_2 sorption experiments at 77 K were carried out on samples previously calcined at 450 °C and outgassed at 250 °C (10^{-4} Pa) with a Micromeritics ASAP 2000 instrument. Specific surface areas were calculated using the BET method. When micropores are present the external surface areas were calculated from the *t*-plot method.

Thermogravimetric/differential thermogravimetric (TG-DTG) experiments were carried out using a Setaram TG-DSC-111 apparatus, with fully programmable heating and cooling sequences, sweep gas valve switchings, and data analysis. The samples were placed in a platinum crucible and dried at 120 °C under He stream (flow: 20 mL min^{-1}). Heating was then performed at 5 °C min^{-1} from RT up to 800 °C in a stream of H_2/Ar (5/95) (flow: 20 mL min^{-1}). The use of a reducing atmosphere aims at studying the reduction process of the samples at increasing temperature.

X-ray diffraction (XRD) patterns were recorded on a Bruker D8 Advance instrument using Cu $K\alpha_1$ radiation ($\lambda = 1.542$ Å, 40 kV and 50 mA) on as-synthesized LDH based samples and on materials first heat-treated at 450 °C in N_2 or air and then at 600 and 1000 °C in H_2.

TEM analysis of the materials was performed using a Jeol 1200 EXII microscope operated at 80 kV on samples previously calcined at 450 °C in N_2 and then reduced at 600 °C. The samples were prepared by suspending and sonicating the reduced catalysts in acetone and placing a drop of the suspension on a carbon copper grid. To obtain the average nickel particle size in surface, $d_S = \sum n_i d_i^3 / \sum n_i d_i^2$, 300–400 particles were measured on representative micrographs.

3. Results and Discussion

3.1. Colloidal Suspensions. The $[Ni(C_6O_7H_3)_x(OH)]_y^{y(3x-1)-}$ colloidal suspensions are clear with no observable turbidity. Their characterizations reveal a negative surface charge of the clusters and a decrease of their size when increasing the [citrate]/[Ni] molar ratio. Colloids with hydrodynamic diameters varying from 7 nm to 1 nm were thus obtained when the Ni complexation ratio increases from 0.5 to 2. The pH of the colloidal suspensions concurrently increases from 9 to 11. Ni colloids then present the right characteristics to be used as intercalate entities between LDH layers: they have a negative surface charge and a small size, and the pH of the suspension lies in the stability range for Mg/Al LDH.

3.2. Materials. *3.2.1. Composition of the Samples.* The elemental analyses reported in Table 1 allow establishing the structural formula of the host structure and the exchanged LDH samples. The metal composition of the host structure is similar to that of the synthesis solution with a Mg/Al molar ratio close to 2 and nitrates as main compensating anions. The composition of Cit-Mg/Al shows that about 50% of the initial nitrates are exchanged by the citrate anions. The Mg/Al ratio in the Cit_xNi-Mg/Al nanocomposites is close to that of the host NO_3-Mg/Al LDH as expected for anion exchanges performed at pH values ranging from 9.5 to 10.5. The carbon content is assigned to the citrate species, though contamination from carbonate ions dissolved in water may occur during exchange experiments performed in air. We already found CO_3^{2-} contamination in similar nanocomposites;[35] however, the materials were obtained by intercalation of controlled smaller amounts of $[Ni(C_6O_7H_3)(OH)]_y^{2y-}$ into the host Mg/Al LDH. In contrast, in the present work, an excess of $[Ni(C_6O_7H_3)_x(OH)]_y^{y(3x-1)-}$ clusters (1.5 times the AEC) was used for intercalation, which is an impediment to the concurrent exchange with carbonates. The exchange of the $[Ni(C_6O_7H_3)_x(OH)]_y^{y(3x-1)-}$ species for nitrates is not complete. The NO_3^- content indeed decreases from 21.0 to 2.5% of the AEC when the $[C_6O_7H_3]$/[Ni] molar ratio in the complexes increases from 0.46 to 1. This is consistent with the concurrent variations of the composition and the mean negative charge of the $[Ni(C_6O_7H_3)_x(OH)]_y^{y(3x-1)-}$ species.

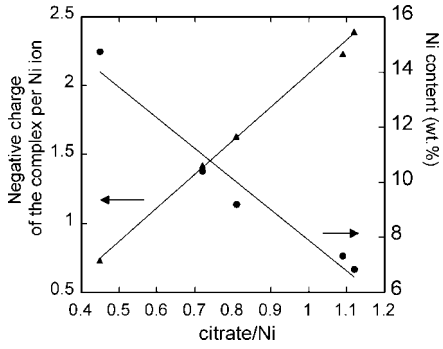

Figure 1. Ni content (wt %) (●) and negative charge of the intercalated Ni hydroxy citrate complex (▲) as a function of the $[C_6O_7H_3]/[Ni]$ molar ratio in the nanocomposites.

After assignment of the citrate content in the $[Ni(C_6O_7H_3)_x(OH)]_y^{y(3x-1)-}$ species, the OH content is determined by assuming charge compensation in the composite samples. The complexation degree ($[C_6O_7H_3]/[Ni]$) in the solids follows the theoretical values in solution and increases until unity, where a plateau is reached. The hydrolysis degree ($[OH]/[Ni]$) concurrently decreases, showing that hydroxylation and complexation phenomena compete in the complexes. A consequence of these variations is that the negative charge of the complexes compulsorily increases from −0.74 in $Cit_{0.5}$Ni-Mg/Al to −2.40 in Cit_1Ni-Mg/Al, that is, when the $[C_6O_7H_3]/[Ni]$ molar ratio increases from 0.46 to 1 (Figure 1). This explains that (i) NO_3^- are extensively exchanged and (ii) the Ni content decreases in the nanocomposites when the complexation degree $[C_6O_7H_3]/[Ni]$ increases (Figure 1). A lower amount of Ni-containing complexes is needed to compensate the layer charge when the negative charge of the guest entities increases. Therefore the composition of the intercalated Ni complex allows controlling the Ni loading in the nanocomposites, which varies from 7 to 15 wt %.

The chemical composition of ClNi-Mg/Al (Table 1) shows that besides $NiCl_4^{2-}$, residual NO_3^- from the host LDH, CO_3^{2-} from contamination, and a particularly large amount of Cl^- are also present. The latter comes from the exchange solution due to the incomplete formation of $NiCl_4^{2-}$ from the reaction of $NiCl_2$ and $(C_2H_5)_4NCl$ and/or some subsequent decomposition of $NiCl_4^{2-}$ as already suggested by Okada et al.[33] The competition between the different anions is unfavorable to $NiCl_4^{2-}$. Consequently the Ni content in the sample does not exceed 3 wt %.

3.2.2. Structural Characterization of the Samples. The XRD patterns of NO_3-Mg/Al and Cit_xNi-Mg/Al nanocomposites are presented in Figure 2. NO_3-Mg/Al exhibits the typical XRD pattern corresponding to a LDH structure. The diffraction peaks can be indexed in a hexagonal unit cell with a $R\bar{3}m$ rhomboedral symmetry generally observed in LDH materials. The sample is highly crystallized with intense and narrow diffraction peaks at below 30° 2Θ, ascribed to (003) and (006) planes. Wide and asymmetric reflections are obtained at higher 2Θ values, as usually observed. The basal spacing $d_{003} = 0.88$ nm is consistent with a Mg/Al ratio of 2 and the presence of NO_3^- as charge compensating anions. Noticeable changes occur in the 2Θ range between 5 and 30° in the XRD patterns of the nanocomposites. The

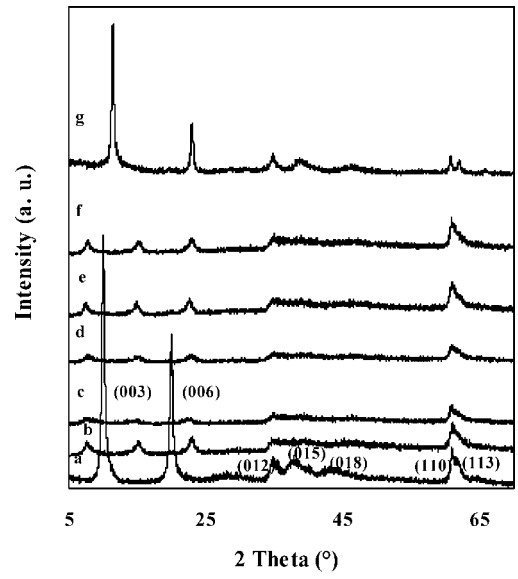

Figure 2. XRD patterns of (a) NO_3-Mg/Al, (b) $Cit_{0.5}$Ni-Mg/Al, (c) Cit_{07}Ni-Mg/Al, (d) Cit_1Ni-Mg/Al, (e) $Cit_{1.5}$Ni-Mg/Al, (f) Cit_2Ni-Mg/Al, and (g) ClNi-Mg/Al.

crystallinity considerably decreases, while three harmonics, that is, the (003), (006), and (009) reflections, are observed. The corresponding basal spacings increase comparatively to the host structure according to the intercalation of the $[Ni(C_6O_7H_3)_x(OH)]_y^{y(3x-1)-}$ species. Moreover they vary from 1.20 to 1.13 nm when the complexation degree increases from 0.5 to 1. This is in agreement with both the decrease of the hydrodynamic size of the colloids in solution and the increase of the mean negative charge of the species which enhances their electrostatic attraction with the layers. In agreement with the chemical analysis, weak Bragg reflections around 10 and 20° 2Θ, which originate from NO_3^- ions, are observed in the XRD patterns of the samples prepared with molar ratios $[C_6O_7H_3]/[Ni] \leq 1$. It must also be pointed out that the (003), (006), and (009) peaks assigned to the LDH structure are shifted and deformed as a result of the intercalation of Ni complexes. This broadening, which is often observed when anionic complexes of large size are intercalated, mainly results from stacking faults of the layers.[12,34,39] Considering the presence of both NO_3^- and $[Ni(C_6O_7H_3)_x(OH)]_y^{y(3x-1)-}$ species, the peak deformation may also be the result of a staging. Second stage intermediates were already observed during the intercalation of carboxylate and phosphonate anions into Li/Al-A^- LDH ($A^- = Cl^-$, Br^-, NO_3^-)[40] and of succinate and tartrate into Zn/Al-Cl or Zn/Cr-Cl LDH.[41] Staging has always been observed when inorganic and organic anions are involved, suggesting that it results from an induced hydrophilic/hydrophobic separation.[41] Regarding Cit_1Ni-Mg/Al, for example, if a second stage intermediate with alternate interlayer spaces containing NO_3^- ($d_{003} = 0.88$ nm) on one hand and $[Ni(C_6O_7H_3)(OH)]^{2-}$ species ($d_{003} = 1.13$ nm) on the other

(39) Li, C.; Wang, G.; Evans, D. G.; Duan, X. *J. Solid State Chem.* **2004**, *177*, 4569.
(40) Williams, G. R.; O'Hare, D. *Chem. Mater.* **2005**, *17*, 2632.
(41) Pisson, J.; Taviot-Guého, C.; Israëli, Y.; Leroux, F.; Munsch, P.; Itié, J. P.; Briois, V.; Morel-Desrosiers, N.; Besse, J. P. *J. Phys. Chem. B* **2003**, *107*, 9243.

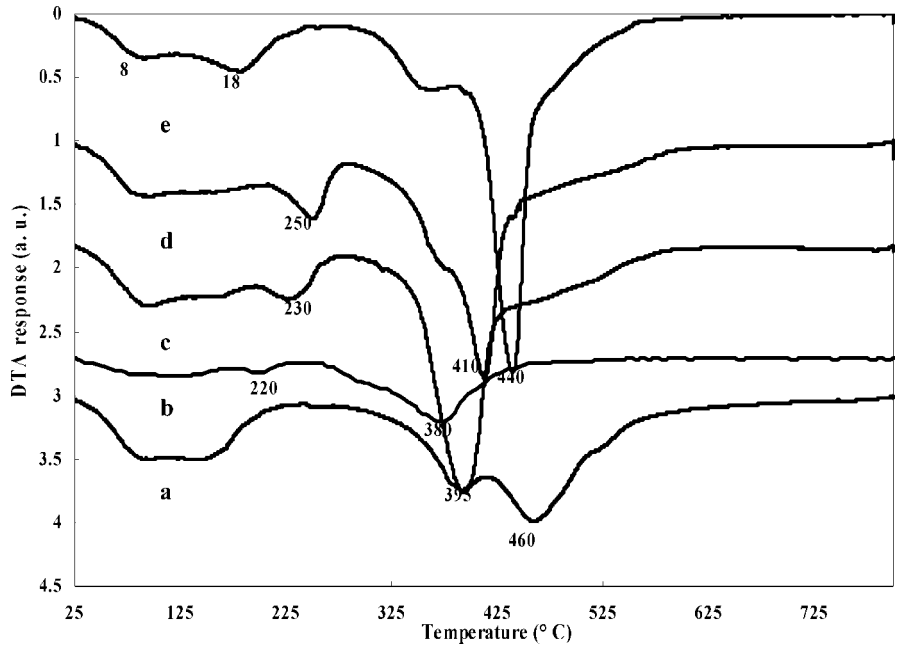

Figure 3. DTG profiles of (a) ClNi-Mg/Al, (b) $Cit_{0.6}$Ni-Mg/Al, (c) Cit_1Ni-Mg/Al, (d) Cit-Mg/Al, and (e) NO_3-Mg/Al under a reducing atmosphere H_2/Ar: 5/95.

hand is present, diffraction peaks should theoretically be detected at $d_{003} = 0.88 + 1.13$ nm $= 2.01$ nm. The presence of (006), (009), and (0015) reflections at *d* spacings of 1.00, 0.67, and 0.40 nm corresponding to a second stage intermediate cannot be totally ruled out considering the broad diffraction lines observed below 30° 2Θ. The lattice parameter *a* ($a = 2d_{110}$) of the Cit_xNi-Mg/Al nanocomposites is similar to that of the NO_3-Mg/Al precursor. As the lattice a parameter corresponds to the intermetallic distance within the brucite-like sheets, its constancy is consistent with similar Mg/Al ratios in these samples (Table 1).

ClNi-Mg/Al exhibits an XRD pattern (Figure 2) with intense and narrow (003) and (006) peaks revealing a higher ordering of the structure. The basal spacing shifts from 0.88 nm to 0.79 nm after exchange in close agreement with the presence of Cl^- as the main compensating anions (Table 1). However, this is also consistent with the concurrent intercalation of $NiCl_4^{2-}$ species as previously reported by Okada et al.[33] in Li/Al-LDH. From EXAFS and ESR experiments, these authors showed that $NiCl_4^{2-}$ has a square planar structure rather than the usual tetrahedral structure, as a result of the strong restriction existing in the interlayer space.

3.2.3. Characterizations of the Reduced Materials. Reduction of Cit_xNi-Mg/Al nanocomposites leads to Mg(Al)O supported Ni^0 particles and is accompanied by structural and textural changes of the materials. These changes were followed with XRD and TG-DTG analyses of $Cit_{0.6}$Ni-Mg/Al, Cit_1Ni-Mg/Al, and ClNi-Mg/Al samples. The influence of the nature (i.e., $NiCl_4^{2-}$ or $[Ni(C_6O_7H_3)_x(OH)]_y^{y(3x-1)-}$) and the composition (*x*: 0.6, 1) of the guest anionic species was examined.

The TG-DTG have been performed in reducing atmosphere (H_2/Ar = 5/95). For the sake of comparison, those of the host NO_3-Mg/Al and of the citrate-exchanged sample Cit-Mg/Al are also given. They show in all cases the characteristic profile of LDH structures exhibiting two different weight loss steps corresponding to the evolution of species (H_2O, CO_2, NO, NO_2) already identified in several papers.[35,42,43] The first continuous weight loss between 20 °C and 300 °C gives rise to two DTG peaks in the case of NO_3-Mg/Al and ClNi-Mg/Al. The first broad peak between 20 and 120 °C, centered at 80 °C, corresponds to removal of water weakly adsorbed on the external surface of the grains. The second broad peak centered at 180 °C is assigned to the release of interlayer water molecules. The corresponding weight loss allows assigning the amount of hydration water in the chemical formula (Table 1). Remarkably, a third intense DTG peak appears with a maximum at 220–230 °C in the Cit_xNi-Mg/Al nanocomposites and at 250 °C in the citrate-exchanged sample (Cit-Mg/Al). It corresponds to a weight loss from 5 to 13%. A similar feature has been previously assigned to the release of constrained water molecules within the domain between grafted organic anions.[44] Then, in the present case, this peak can tentatively be assigned to the release of water molecules associated with citrates as compensating anions or Ni complexing species. A second weight loss with a DTG broad peak extending from 250 to 800 °C is observed in all samples. It corresponds to dehydroxylation of the layers and decomposition of the intercalated anionic species. These weight losses, amounting 32 to 36 wt %, are below the theoretical value of 40–48 wt % showing that dehydroxylation of the layers is initiated before 250 °C. The maximum temperatures of decomposition are recorded at 440, 410, 395, and 380 °C for NO_3-Mg/Al, Cit-Mg/Al, Cit_1Ni-Mg/Al, and $Cit_{0.6}$Ni-Mg/Al, respectively. Therefore, NO_3^- and citrate anions interact more strongly

(42) Hibino, T.; Yamashita, Y.; Kosuge, K.; Tsunashima, A. *Clays Clay Miner.* **1995**, *43*, 427.
(43) Rives, V. *Inorg. Chem.* **1999**, *38*, 406.
(44) Li, F.; Zhang, L.; Evans, D. G.; Forano, C.; Duan, X. *Thermochim. Acta* **2004**, *424*, 15.

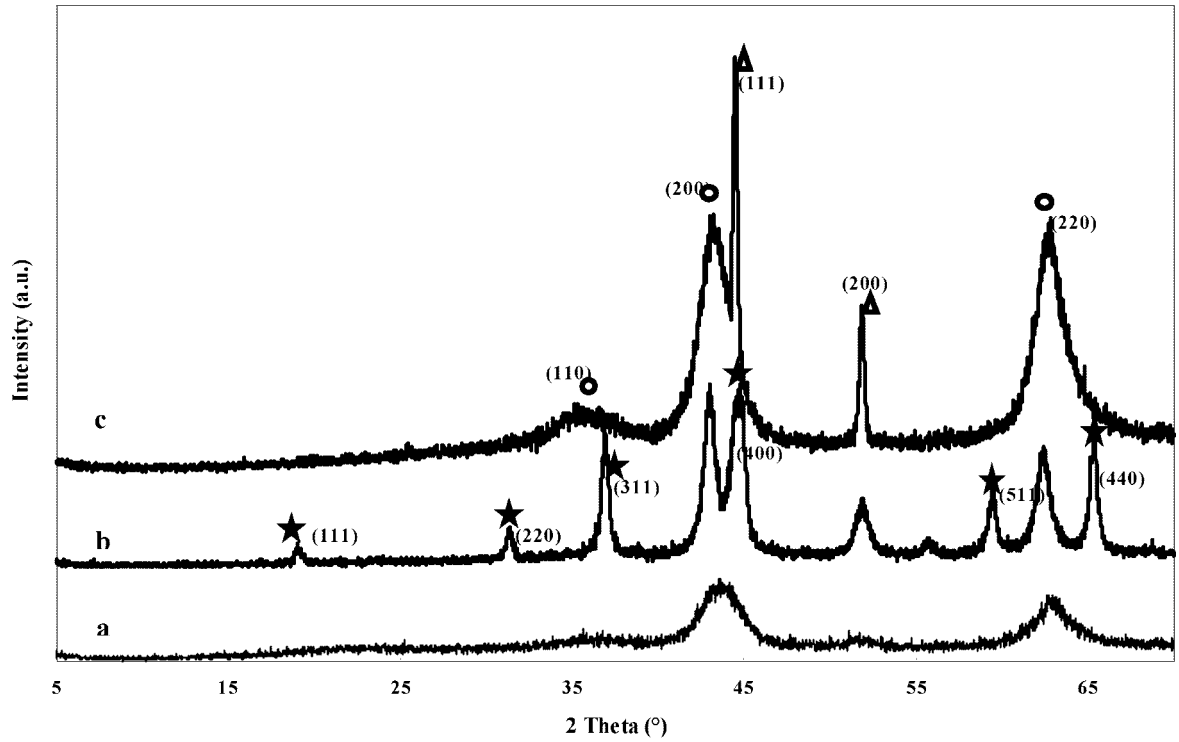

Figure 4. XRD patterns of (a) Cit_1Ni-Mg/Al reduced at 600 °C, (b) Cit_1Ni-Mg/Al reduced at 1000 °C, and (c) ClNi-Mg/Al reduced at 800 °C under H_2 (H_2/N_2: 25/75; △, Ni^0; ★, spinel phase; ○, mixed oxide).

with brucite-like layers than $[Ni(C_6O_7H_3)_x(OH)]_y^{y(3x-1)-}$. Besides, the decomposition temperature of the $[Ni(C_6O_7H_3)_x(OH)]_y^{y(3x-1)-}$ clusters decreases when their negative charge decreases. This is also in agreement with the concurrent weakening of the electrostatic interaction with the brucite-like layers. Decomposition of NO_3^- present in the nanocomposites is probably made easier by the presence of Ni ions.

In contrast with the previous materials, the TG-DTG curve of ClNi-Mg/Al exhibits a broad DTG peak with a maximum at 460 °C and a shoulder at 395 °C. Similar features were already assigned to dehydroxylation of the layers in the case of Li/Al LDH intercalated with $NiCl_4^{2-}$ and NO_3^-, respectively.[33] The chemical composition of ClNi-Mg/Al (Table 1) likely suggests that these peaks are due to the release of HCl formed by decomposition of $NiCl_4^{2-}$ and Cl^- anions.

An interesting feature is observed when comparing the TG profiles of all samples. The mass losses above 450 °C for Cit_1Ni-Mg/Al and ClNi-Mg/Al of 13.8 and 8.4%, respectively, are significantly higher than those of Cit-Mg/Al and NO_3-Mg/Al, of 5.6 and 3.5%, respectively. This shows that in the former samples, complete decomposition of anions can only be achieved at a higher temperature in spite of the lower interaction of the intercalated species with the brucite-like layers.

Total weight losses of approximately 45% for ClNi-Mg/Al and 50–54 wt % for the citrate-containing LDH (Cit_xNi-Mg/Al and Cit-Mg/Al) agree with the expected values from the structural formula. Consequently the Ni loading in the Ni/Mg(Al)O materials obtained from activation of Cit_xNi-Mg/Al precursors ranges from 14.5 to 29.5 wt %.

The powder XRD patterns of all materials treated first at 450°C in N_2 and then at 600 °C in H_2/Ar (5/95) are characteristic of a poorly crystallized rock-salt periclase type Mg(Al)O phase (Figure 4). They indeed exhibit the peaks assigned to the (110), (200), and (220) planes, at approximately 37°, 43°, and 62° 2Θ, respectively. Moreover, in the case of the Ni-containing samples, the (200) peak at 43° 2θ assigned to Mg(Al)O is broadened because of its overlap with the (111) peak of Ni^0. It is worth noting that the crystallinity of the Ni^0 phase is considerably higher in ClNi-Mg/Al than in the Cit_xNi-Mg/Al samples. When the reduction temperature increases up to 1000 °C, intense new peaks appear located at 31.30°, 36.90°, 44.75°, 59.44°, and 65.35° 2Θ; they are assigned to (220), (311), (400), (511), and (440) reflections of the $MgAl_2O_4$ spinel-like phase, which coexists with the rock-salt-like structure. At 1000 °C, the Ni^0 phase becomes highly crystallized, as shown by sharp and intense reflections.

As expected the mean size of the Ni^0 crystallites varies with the reduction temperature, but most interestingly with the composition of the guest entities in the nanocomposites. The estimated Ni^0 crystallite coherent sizes were determined using the Scherrer equation from the line broadening of the (200) diffraction peak at ∼52° 2θ rather than from the most intense (111) peak, which overlaps with the (200) peak of Mg(Al)O. After reduction at 600 °C, the crystallite sizes are approximately 10.5 and 8.20 nm for $Cit_{0.6}Ni$-Mg/Al and Cit_1Ni-Mg/Al, respectively. Therefore they decrease when the Ni complexation degree (the $[C_6O_7H_3]/[Ni]$ molar ratio) in the Cit_xNi-Mg/Al nanocomposites increases. After reduction at 1000 °C, the mean Ni^0 crystallite sizes increase to

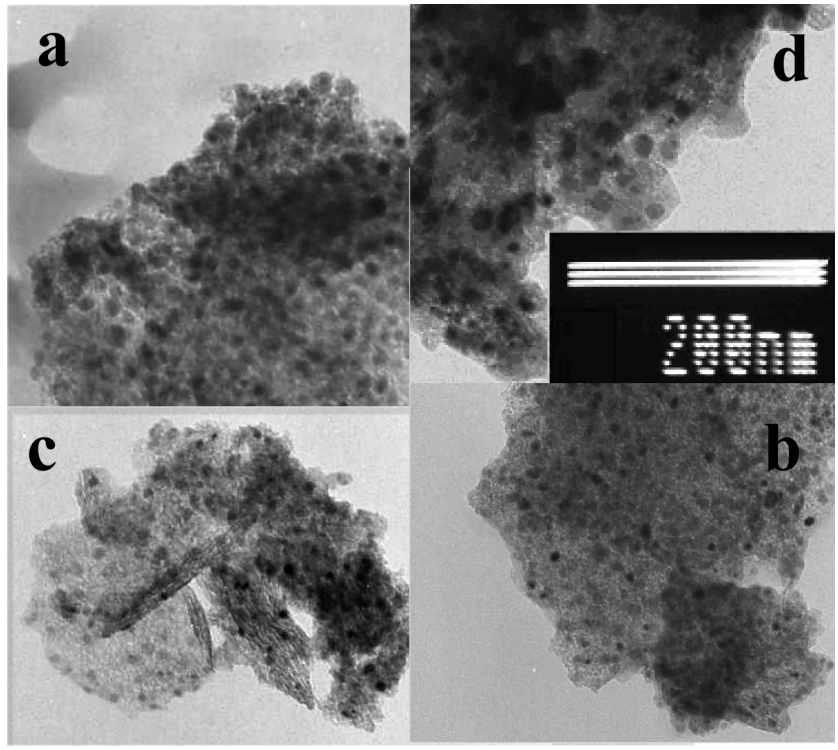

Figure 5. TEM images of samples (a) Cit_{06}Ni-Mg/Al, (b) Cit_1Ni-Mg/Al, (c) Cit_2Ni-Mg/Al heat treated under N_2 at 450 °C and then reduced at 600 °C under H_2, and (d) $Cit_{0.6}$Ni-Mg/Al heat treated under N_2 at 450 °C and then reduced at 1000 °C under H_2.

approximately 24.7 nm and 18.5 nm for $Cit_{0.6}$Ni-Mg/Al and Cit_1Ni-Mg/Al, respectively, as a result of particle sintering (Figure 4). In agreement with the higher crystallinity of the Ni^0 phase in the nanocomposites obtained by intercalation of $NiCl_4^{2-}$ entities, the mean crystallite size reaches 61.5 nm after reduction at 800 °C of ClNi-Mg/Al. In that case, sintering of the particles is particularly enhanced in comparison with the Cit_xNi-Mg/Al nanocomposites, although the Ni loading in this sample is much lower (Table 1). Larger crystallite sizes are also obtained when Cl^- instead of CO_3^{2-} or NO_3^- are the compensating anions in multicationic Ni/Mg/Al LDH.[45] In the nanocomposites, the carbon-rich protecting shells formed by decomposition of the citrate species in the Cit_xNi-Mg/Al samples comparatively to ClNi-Mg/Al play a major role and allow the sintering of the Ni^0 particles to be inhibited.[35]

A prior calcination at 450 °C in air of Cit_1Ni-Mg/Al leads to crystallite coherent sizes of 12.4 and 23 nm after reduction at 600 and 1000 °C, respectively. This corresponds to a 30–50% increase of size in comparison with calcination-free materials (vide supra). This feature accounted for the exothermic decomposition of citrate species, as they contain three carboxylate groups that give high amounts of CO_2 and contribute to particle sintering.[35]

An increase of the specific surface area is observed from 101 $m^2\ g^{-1}$ in the host NO_3-Mg/Al to 270−330 $m^2 g^{-1}$ in the Cit_xNi-Mg/Al nanocomposites. As expected the specific surface areas of the nanocomposites decrease after reduction. It is due to the formation of the different crystalline phases and to the increase of crystallinity with temperature. For example for Cit_1Ni-Mg/Al heat treated at 450 °C in nitrogen, the specific surface area decreases from 280 $m^2\ g^{-1}$ to 224 and 59 $m^2\ g^{-1}$ after reduction at 600 and 1000 °C, respectively.

To sum up, to achieve a high Ni dispersion after reduction at high temperature (i) Ni colloids formed by hydrolysis of Ni cations in the presence of strong complexing agents (e.g., citrate anions) are more suitable than $NiCl_4^{2-}$ complexes as guest species of the nanocomposites and (ii) the composition of the Ni hydroxy citrate colloids is the relevant parameter. The carbon-rich shell coating around the Ni particles provided by the decomposition of the citrate of the complexes slows down the sintering.

TEM images of reduced $Cit_{0.6}$Ni-Mg/Al, Cit_1Ni-Mg/Al, and Cit_2Ni-Mg/Al samples are reported on Figure 5. To achieve decomposition of the citrate species prior to the reduction treatment, the samples were first heat-treated at 450 °C in nitrogen. In a previous study, it was indeed shown that the thermal treatment leads to a narrower size distribution of the Ni particles when performed in nitrogen instead of air.[35] $Cit_{0.6}$Ni-Mg/Al reduced at 600 °C shows a broad particle size distribution ranging from approximately 2.8 to 16 nm with an average size of 10 nm. A narrower distribution is reached in the case of Cit_1Ni-Mg/Al or Cit_2Ni-Mg/Al also reduced at 600 °C; the two samples are very similar, which is expected because the LDH composite precursors have the same compositions (similar citrate/Ni ratios close to 1, in the solids). The Ni particle size distribution ranges from approximatively 3 to 7 nm with a mean size of 5 nm in both cases. Moreover, in both samples, some Ni particles aligned and probably embedded in crystallites exhibiting platelet morphology are clearly distinguished. Those particles present an average size of 2.4 nm; the plate-like morphology of the

(45) Lebedeva, O.; Tichit, D.; Coq, B. *Appl. Catal., A* **1999**, *183*, 61.

material corresponds to that of the Mg(Al)O mixed oxide particles retaining the general habit of the LDH precursor. LDH structures are indeed topotactically decomposed upon thermal treatment as previously reported for Mg/Al[46] and Ni/Al LDH.[47,48] The comparison of the previous results shows that an increase of the complexation degree of Ni^{2+} by citrate anions allows the average particle size to be decreased and the size distribution to be narrowed. The size of the particles increases after reduction at 1000 °C as shown for Cit_1Ni-Mg/Al. The mean Ni particle size reaches 15 nm. Therefore a complete decomposition of the citrate species as well as the total reduction of NiO obtained at high temperature leads to sintering of the Ni particles with a broadening of their size distribution. The average particle size determined by TEM is in all cases smaller than the average crystallite size from XRD data. This is quite normal because the particle size derived from the Scherrer formula should be compared with the mean volume diameter $d_v = \sum n_i d_i^4 / \sum n_i d_i^3$ from TEM, which is always shifted to higher values than the mean number diameter $d_s = \sum n_i d_i^3 / \sum n_i d_i^2$, which is actually calculated. However, the low crystallinity of the samples reduced at 600 °C can lead to a discrepancy between the particle sizes and the coherent domains.

3.2.4. Reconstruction of the Materials. Mg(Al)O mixed oxides calcined below 800 °C exhibit XRD patterns similar to those of a mixed-rock-salt phase. However, it deviates from the idealized phase because of a partial substitution of aluminum for magnesium and the presence of a supercell giving rise to a defective spinel-like structure.[47,49,50] The layered structure is restored upon dispersion in water containing carbonate or other anions. Several reports establish that Mg/Al-LDH reconstruction proceeds through a dissolution−reprecipitation process.[38,51,52] Accordingly, when Mg(Al)O is dispersed in an aqueous solution containing some divalent cations (Zn^{2+}, Ni^{2+}, Co^{2+}, Cu^{2+}), the latter are incorporated within the layers.[51,52] Another evidence of this process is that a mixture of MgO and Al_2O_3 soaked in an aqueous solution of Na_2CO_3 yields an LDH-type phase.[53] A main consequence of this is that the reconstruction process depends on the solubility of the divalent metal hydroxide in water.[53] This fact and the high degree of inversion explain the poor reconstruction of the defective spinel-like structures obtained by calcination of Ni/Al and Ni/Mg/Al LDH.[36,48] When Mg/Al LDH are decomposed at 1000 °C, crystallization of the highly stable $MgAl_2O_4$ spinel phase hinders LDH reconstruction. However, reconstruction has been reported for the unstable inverse spinel phases obtained by calcination at a moderate temperature of a Cu-Co-Zn-Al LDH due to a retro-topotactic transformation.[54]

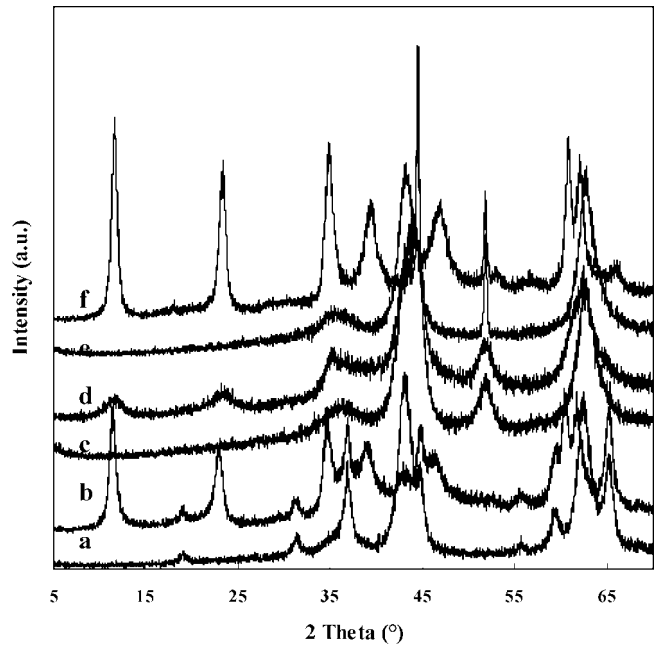

Figure 6. XRD patterns of (a) Cit-Mg/Al reduced at 1000 °C, (b) sample (a) after rehydration, (c) Cit_1Ni-Mg/Al reduced at 800 °C, (d) sample (c) after rehydration, (e) ClNi-Mg/Al reduced at 800 °C, and (f) sample (e) after rehydration.

In the present study, the NO_3-Mg/Al and Cit-Mg/Al LDHs reduced at 1000 °C give a mixture of Mg(Al)O, $MgAl_2O_4$, and Ni^0 phases. By dispersion in water (2 h at RT), reconstitution of the LDH phase takes place by transformation of the Mg(Al)O phase only, whose (200) and (220) XRD peaks vanish, while those of the $MgAl_2O_4$ phase show no significant change (Figure 6). A similar behavior was reported in the literature for a Mg/Al LDH calcined at 950 °C and then dipped in a Ni^{2+} nitrate aqueous solution. The Mg(Al)O phase was converted into Mg(Ni)-Al LDH, while $MgAl_2O_4$ spinel did not show any transformation.[38] The interlayer distance $d_{003} = 0.77$ nm of the regenerated NO_3-Mg/Al and Cit-Mg/Al LDH is in agreement with the intercalation of CO_3^{2-} dissolved in water. The nanocomposites behave differently from the host structure upon reconstruction treatments. This is more clearly put in evidence on the samples reduced at 800 °C, which are composed of Ni^0 supported on the Mg(Al)O phase. ClNi-Mg/Al indeed shows a reconstitution of the LDH phase from the support, but in contrast, reconstruction scarcely occurs for Cit_1Ni-Mg/Al (Figure 6). An increase up to 24 h of the rehydration time does not significantly increase the fraction of reconstructed LDH, showing that it is not kinetically limited. As shown by XRD characterizations of all samples, the Ni phase is not affected by reconstruction.

The host structure and the ClNi-Mg/Al nanocomposite treated in reducing atmosphere show a similar and high reconstruction ability of the Mg(Al)O mixed oxide support, whereas it is highly stabilized when the precursors are Cit_xNi-Mg/Al nanocomposites. TPR experiments have shown that

(46) Abelló, S.; Medina, F.; Tichit, D.; Pérez-Ramírez, J.; Groen, J. C.; Sueiras, J. E.; Salagre, P.; Cesteros, Y. *Chem. Eur. J.* **2005**, *11*, 728.
(47) Clause, O.; Rebours, B.; Merlen, E.; Trifirò, F.; Vaccari, A. *J. Catal.* **1992**, *133*, 231.
(48) Prinetto, F.; Tichit, D.; Teissier, R.; Coq, B. *Catal. Today* **2000**, *55*, 103.
(49) Fornasari, G.; Gazzano, M.; Matteuzzi, D.; Trifirò, F.; Vaccari, A. *Appl. Clay Sci.* **1995**, *10*, 69.
(50) Gazzano, M.; Kagunya, W.; Matteuzzi, D.; Vaccari, A. *J. Phys. Chem. B* **1997**, *101*, 4514.
(51) Stanimirova, T.; Kirov, G. *Appl. Clay Sci.* **2003**, *22*, 295.
(52) Stanimirova, T.; Kirov, G. *J. Mater. Sci. Lett.* **2001**, *20*, 453.
(53) Rajamathi, M.; Nataraja, G. D.; Ananthamurthy, S.; Kamath, P. V. *J. Mater. Chem.* **2000**, *10*, 2754.
(54) Marchi, A. J.; Apesteguía, C. R. *Appl. Clay Sci.* **1998**, *13*, 35.

reduction is complete at 780 °C with an H_2 uptake corresponding to the stoichiometric reduction of Ni^{2+} into Ni^0.[35] This is consistent with TG-DTG results under H_2 and the detection of Ni^0 particles by XRD due to Ni^0 segregation. Therefore in the reduced Cit_xNi-Mg/Al samples we can suggest that LDH reconstruction is prevented accounting for an interaction between the Ni^0 particles and the Mg(Al)O support and/or for a low accessibility of water due to the embedded Ni particles, put in evidence by TEM. In contrast, reconstruction significantly occurs when very large Ni^0 particles are formed in reduced ClNi-Mg/Al samples. An extended segregation of the large Ni^0 particles toward the outershell of Mg(Al)O grains makes easier the reconstitution of the LDH phase from the mixed oxide.

4. Conclusion

Ni nanoparticles supported on Mg(Al)O mixed oxide have been obtained from a series of nanocomposites prepared by anionic exchange of Mg/Al LDH host structures with $[Ni(C_6O_7H_3)_x(OH)]_y^{y(3x-1)-}$ clusters of varying composition. The study follows a previous work[35] where the Ni loading was controlled through the exchange degree with the same colloid of fixed composition $[Ni(C_6O_7H_3)(OH)]_y^{2y-}$ of the host Mg/Al LDH. In the present work the composition of the nanocluster was varied to finely control both the Ni loading and the size of the particles after reduction. For this purpose the $[C_6O_7H_3]$/[Ni] molar ratio in the colloids was increased from 0.5 to 2. This leads to an increase of their negative charge with a concurrent decrease from 7 nm to about 1 nm of their hydrodynamic size. According to the variation of charge, the exchange of $[Ni(C_6O_7H_3)_x(OH)]_y^{y(3x-1)-}$ for NO_3^- is better achieved at higher $[C_6O_7H_3]$/[Ni] molar ratios. Another consequence is that the Ni content in the Ni-Mg/Al LDH nanocomposites decreases from 15 to 7 wt % when the $[C_6O_7H_3]$/[Ni] molar ratio increases from 0.5 to 1 as a result of the increase of the negative charge. This series of nanocomposites leads to a two times increase of the Ni content previously reached by varying the exchange ratio. The relevant feature is that the composition and the size of the intercalated $[Ni(C_6O_7H_3)_x(OH)]_y^{y(3x-1)-}$ species allow tuning the mean size and distribution of the Ni^0 particle in the reduced samples. The mean particle size determined by TEM after reduction at 600 °C indeed decreases from 10 to 5 nm when the $[C_6O_7H_3]$/[Ni] molar ratio increases from 0.6 to 1 in the nanocomposite, and concurrently the Ni^0 content varies from 29.5 to 14.5 wt %. To control the size and the content of Ni^0 particles, the intercalation of hydrolysis products of Ni^{2+} with carboxylic complexing agents like citrates is more efficient than the intercalation of halide (Cl^-) complexed species, such as $[NiCl_4]^{2-}$, which leads to larger particles. The reconstruction ability of the Mg(Al)O mixed oxide almost disappears when it is the support of the Ni^0/Mg(Al)O samples obtained by reduction of the $[Ni(C_6O_7H_3)_x(OH)]_y^{y(3x-1)-}$-Mg/Al LDH nanocomposites. This can be assigned to a strong interaction between the support and the embedded Ni^0 particles. This property is of great interest for catalytic applications requiring a structural stability of the material, particularly those performed in an aqueous medium.

CM071194L